

OPTICAL AND H I STUDIES OF THE "GAS-RICH" DWARF IRREGULAR GALAXY DDO 154

CLAUDE CARIGNAN^{1,2} AND SYLVIE BEAULIEU

Département de physique and Observatoire astronomique du Mont Mégantic, Université de Montréal

Received 1989 April 7; accepted 1989 June 17

ABSTRACT

A study of the luminous and dark components of the dwarf irregular galaxy DDO 154 is presented. From the surface photometry, a scale length $\alpha^{-1} = 0.5$ kpc and a central surface brightness $B(0)_c = 23.17$ are derived for the stellar disk with mean colors typical of Im galaxies. The photometry of the brightest blue stars, combined with the likely association with the CVn I cloud, suggest a distance $\Delta \leq 4.0$ Mpc.

DDO 154 is one of the most gas-rich galaxy known with $(M_{\text{HI}}/L_B) = 5.4$. The H I disk reaches nearly 5 Holmberg diameters (D_{Ho}). From the very regular velocity field, the rotation curve is derived unambiguously out to 15 optical scale lengths. There is a clear flattening of the rotation curve for $r > 4'$ and an indication that it may be declining in the very outer parts.

The shape of the rotation curve, and the fact that for $r > 2$ kpc it is completely dominated by the dark component, allow one to constrain almost uniquely the parameters of the mass model. The final model has $(M/L_B)_* = 1.0 (M_\odot/L_\odot)$ for the stellar disk, a core radius $r_c = 3.0$ kpc, and a central density $\rho_0 = 0.015 M_\odot \text{pc}^{-3}$ for the dark isothermal halo. At the last observed point ($r = 7.6$ kpc), more than 90% of the mass is dark.

Subject headings: galaxies: individual (DDO 154) — galaxies: internal motions —
galaxies: interstellar matter — galaxies: photometry radio sources: 21 cm radiation

I. INTRODUCTION

About ten years ago, Rubin, Ford, and Thonnard (1980), in their classical paper on optical rotation curves of Sc galaxies, asked a series of questions which stressed the importance of studying dwarf galaxies.

Does the common form for the Sc rotation curves mean that all Sc galaxies, small or large, sit in generally similar potential wells, in which the optical galaxy defines only that region in which matter happens to be luminous? If we could observe beyond the optical image, especially for the *smaller galaxies*, would the velocities continue to rise, following the curve defined by those galaxies whose luminous matter extends to much larger nuclear distances? *Is the luminous matter only a minor component of the total galaxy mass?* Observations of neutral hydrogen may enable such questions to be answered.

In recent years, we have concentrated our efforts at studying the mass distribution of late-type spirals (Carignan and Freeman 1985; Carignan 1985; Carignan, Sancisi, and van Albada 1988). The main question those studies were trying to answer was: "Do the properties of dark matter vary as a function of galaxy mass and/or luminosity?"

So far, for galaxies covering a wide range in luminosities ($-21 \leq M_B \leq -16$), no real variation was seen: the central densities of dark halos are a few $\times 10^{-3} M_\odot \text{pc}^{-3}$, and the ratio $M_{\text{dark}}/M_{\text{lum}} = 1.1 \pm 0.5$ at the Holmberg radius (Carignan 1987). At the last observed point of the rotation curves, this ratio reaches 2-3. One question we want to address

is whether this apparent constancy in the properties of dark matter extends all the way down to the low-luminosity, less massive systems. However, in order to be able to see significant trends in such important quantities as the central densities of halos and $M_{\text{dark}}/M_{\text{lum}}$, a homogeneous sample with H I rotation curves, full tilted-ring model analysis of the velocity fields, and similar mass modeling techniques need to be assembled.

The interest for studying dwarf irregulars comes also from the fact that they may be the most common type of objects in the universe. Recent studies by Tyson (1988) and Tyson and Scalo (1988) suggest that there may exist a large population of gas-rich dwarf irregular galaxies. This population could, among other things, explain the fact that the high column density ($N_{\text{HI}} \geq 10^{20} \text{cm}^{-2}$) systems seen in QSO spectra (Wolfe *et al.* 1986) appear 5 times more frequently than can be accounted for by the observed number density and sizes of "normal" gas-rich galaxies. Their "bursting dwarf galaxy" model suggests that a large fraction of these dwarfs remains undetected due to observational selection effects (angular diameter, surface brightness). Dekel and Silk (1986), in their cold dark matter biased galaxy formation picture, also predict that the universe is more uniformly filled with dwarf galaxies than with big ones. We propose that DDO 154 could be a prototype of such a gas-rich low surface brightness small optical diameter galaxy which happens to be relatively nearby. This does not mean to say that most undetected dwarfs are as gas-rich as DDO 154, which is probably an extreme case. For example, in the Virgo cluster, many low surface brightness dwarfs were not detected at H I (Hoffman, Helou, and Salpeter 1988), implying a low gas content.

The unusual H I properties of DDO 154 were discovered serendipitously by Krumm and Burstein (1984) at the Arecibo Observatory and confirmed later by Hutchmeier and Seiradakis (1985). While those two studies were able to show that the H I could be traced out to several optical radii and that the H I mass-to-light ratio of this system was exceptionally large,

¹ Visiting Astronomer, Very Large Array, National Radio Astronomy Observatory, operated by Associated Universities, Inc., under contract with the National Science Foundation.

² Visiting Astronomer, Kitt Peak National Observatory, National Optical Astronomy Observatory, operated by AURA, Inc., under contract with the National Science Foundation.

the data were of to low resolution to be able to extract valuable information from the kinematics. We thus decided to observe DDO 154 in the 21 cm H I line with the Very Large Array (VLA) and in the optical with the 1.6 m telescope of l'Observatoire astronomique du Mont Mégantic (OAMM) and the No. 1 0.9 m telescope of Kitt Peak National Observatory (KPNO). A *B* and an *R* frame obtained at KPNO are shown in Figure 1 (Plate 9).

A discussion on the dark content of this dwarf galaxy was given previously (Carignan and Freeman 1988). In this paper, we want to discuss in much more detail the optical and radio observations (§ II), the light distribution (§ III), the H I properties and kinematics (§ IV), and the mass distribution (§ V). A summary of the results and the conclusions are given in § VI.

II. OBSERVATIONS

a) Optical

The *BVR* optical data using an RCA thinned CCD were obtained during three observing runs: in 1986 February and 1987 April at OAMM and also in 1986 February at KPNO. With 30 μm pixels, the resolution was 0".48 per pixel for a total field of 4.1 \times 2.6 at OAMM and 0".86 per pixel for a field of 7.3 \times 4.6 at KPNO. The readout noise was $\sim 55e^-$ for the OAMM CCD and $\sim 75e^-$ for the KPNO instrument.

Typical seeing (FWHM) for these runs was ~ 1.8 arcsec at OAMM and better than 1.0 arcsec at KPNO. However, the KPNO values may be underestimated due to the large pixel size. The integration times were 1800 s for all the filters at OAMM, 1800 s in *B*, and 900 s in *V* and *R* at KPNO. For those observations, the magnitude scales were determined by observing a standard field in M67 (Schild 1983).

The optical data will serve two purposes: to derive the total luminosity profile that will be used for the study of the mass distribution in § V, and to get the magnitudes of the brightest blue stars (easily resolved in Fig. 1) that will be used as one of the distance indicators for DDO 154.

b) Radio

DDO 154 was observed at the VLA on 1985 November 23. During the 12 hr run, 9.5 hr were spent integrating on source while the remainder went into observing the phase calibrator 1252 + 119 every half-hour and the flux calibrator 3C 286 for 15 minutes. Since the large extent of the H I was known from the Arecibo data (Krumm and Burstein 1984), and since maximum sensitivity was needed, the D-configuration was used with 25 antennas. The parameters of the observations can be found in Table 1.

The total bandwidth of 1.56 Mhz was divided into 32 channels with the first channel being replaced by a "pseudo-continuum" channel. This leaves 31 line channels with a channel separation of 48.8 kHz which corresponds to a velocity of 10.31 km s⁻¹. For these observations, the band was centered at an heliocentric radial velocity $V_{\odot} = 375$ km s⁻¹.

For the pre-treatment of the data, the VLA DEC-10 computer and NRAO standard programs were used. The data were first examined carefully in the (*u-v*)-plane for bad points due to either interference or crosstalk between antennas. When identified, those individual antennas or baselines were flagged for the corresponding integration. Similarly, the antennas which suffered from shadowing either at the beginning or at the end of the observations were eliminated for those periods. The data

TABLE 1
PARAMETERS OF THE VLA OBSERVATIONS

Parameter	Value
Date of observation (12 hr)	1985 Nov 23
Primary beam at half-power (FWHM)	$\sim 32''$
FWHM of synthesized beam	33.5" \times 35.3"
Total bandwidth	1.56 Mhz
Central velocity, heliocentric	375 km s ⁻¹
Number of channels	31
Channel width	10.31 km s ⁻¹
rms noise in channel maps (full resolution)	1.5 mJy per beam
Conversion factor, equivalent	
1 mJy per beam area	
45" \times 45" beam	0.30 K
60" \times 60" beam	0.17 K
Maps gridding	10" \times 10" pixels; uniform weighting; no taper

were then calibrated using the standard VLA calibration procedure.

Once calibrated, the UV data were processed through the VLA PIPELINE system to produce 31 line maps using uniform weighting and no taper. The data were gridded in 10" \times 10" pixels. The resulting beam was 33".5 \times 35".3 and the rms noise in each channel map of the full resolution data was 1.5 mJy per beam.

DDO 154 was also observed for another 12 hr period on 1985 November 22. Both sets of data were calibrated separately and maps produced with the intention of combining them in the map plane (because of insufficient disk space to combine them in the [*u-v*]-plane). However, the November 22 observation suffered from many problems which, even after careful editing of the raw data, produced maps of much lower quality. Not only were the data noisier, but because many baselines had to be rejected (especially short ones), a large fraction of the total flux was missing. The result was that the combined maps were of lower quality than the November 23 data alone. We thus decided not to use the November 22 observation.

Inspection of the individual maps showed that the first and last nine channels were free of line emission. They were averaged together to form the continuum map which is shown in Figure 2 (Plate 10). No strong continuum emission is seen from DDO 154 besides weak emission at a 2 σ level (1.0 mJy per beam) coincident with an H II region. Numerous background point sources can be seen in the field. Profiles at the positions of each of them were examined for possible H I absorption but none could be seen. This map also revealed the head-tail source associated with the elliptical galaxy NGC 4789. Finally, after subtracting the averaged continuum from the line channels, the maps were CLEANed separately and restored with a circular Gaussian beam of 45". Another data cube with 60" resolution was also created to bring out the large-scale structure.

III. OPTICAL STUDIES

a) Surface Photometry

The isophote map and the fitted ellipses down to a level of $\mu_B = 26.5$ mag arcsec⁻² are shown in Figure 3. The parameters of the ellipses can be found in Table 2. We see that there is a regular displacement of the centroid of the isophotes toward

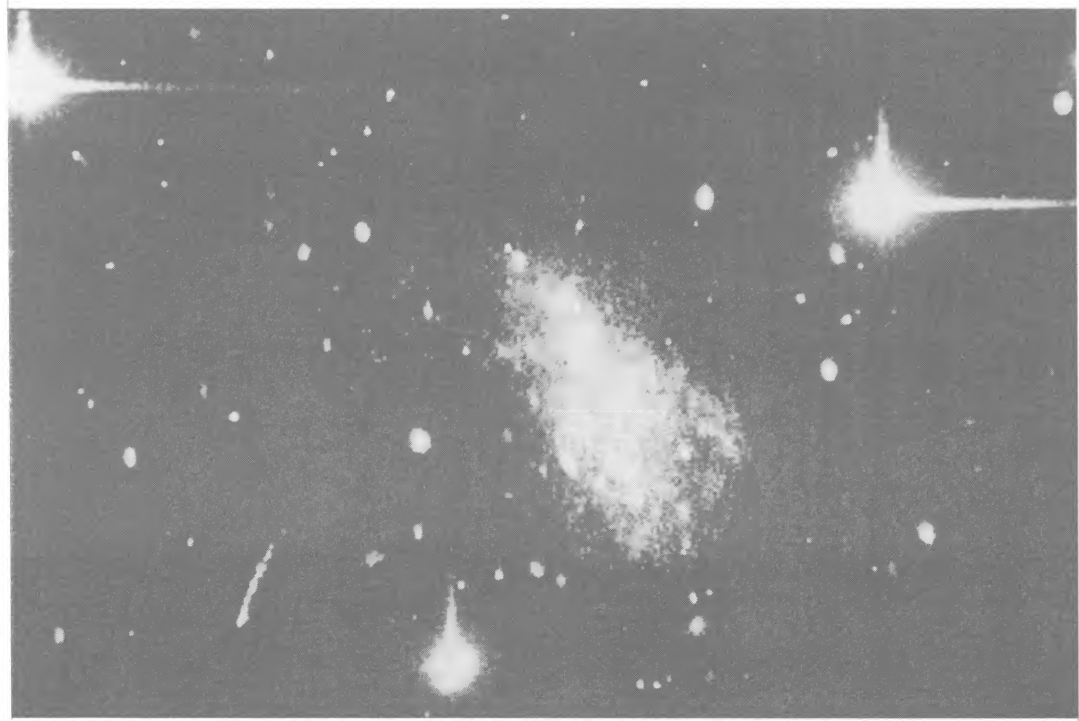


FIG. 1.—Prints of a *B* (top) and an *R* (bottom) CCD frame from KPNO. Note how the brightest stars are well resolved.

CARIGNAN AND BEAULIEU (see 347, 761)

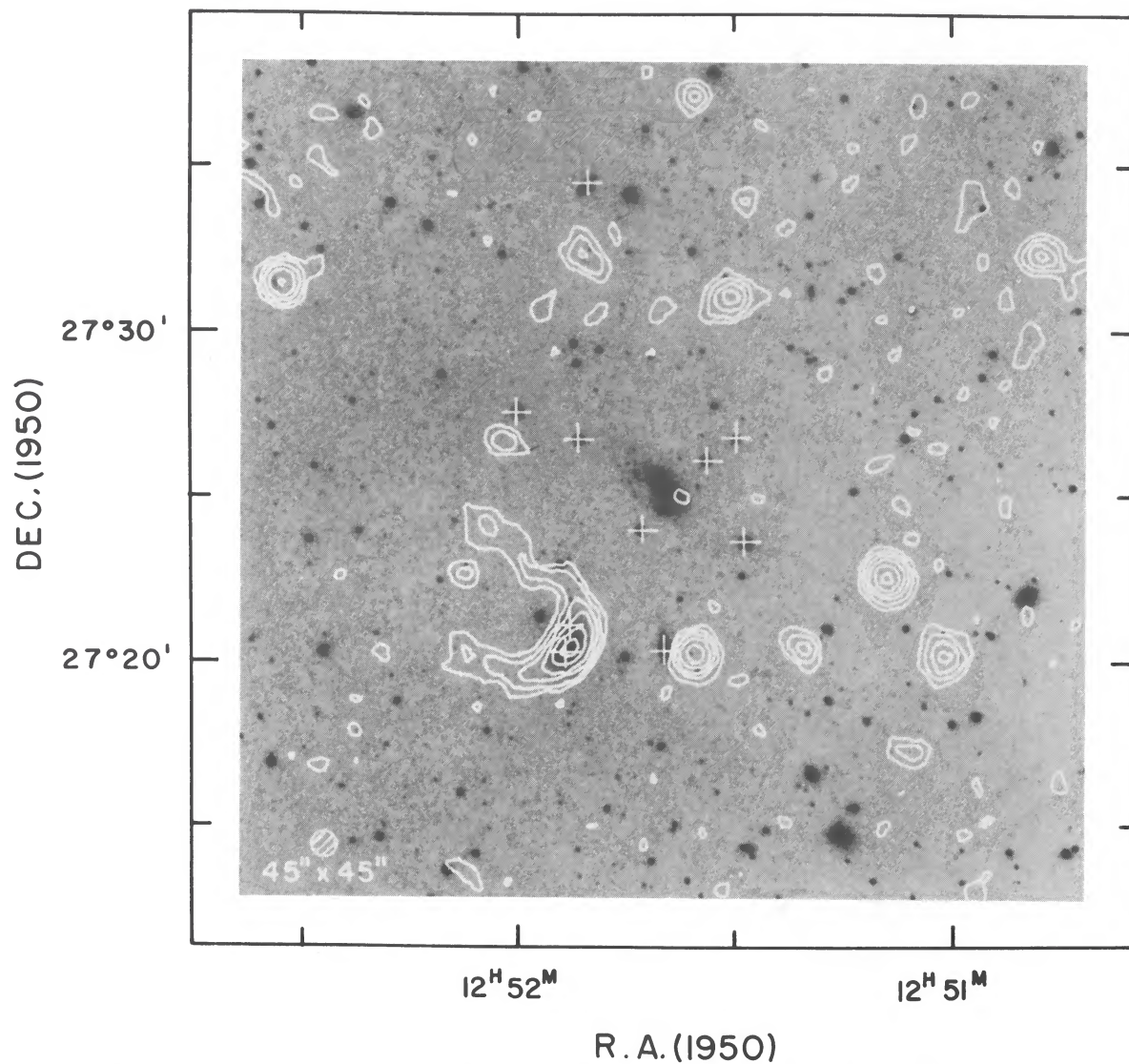


FIG. 2.—Contour diagram of the 21 cm continuum radiation (sum of 18 channels) superposed on the optical (© 1960 National Geographic Society, Palomar Observatory Sky Survey. Reproduced by permission of the California Institute of Technology). Note the head-tail source NGC 4789. The contours are for 1, 2, 4, 8, 16, 32, 64 mJy per beam.

CARIGNAN AND BEAULIEU (see 347, 761)

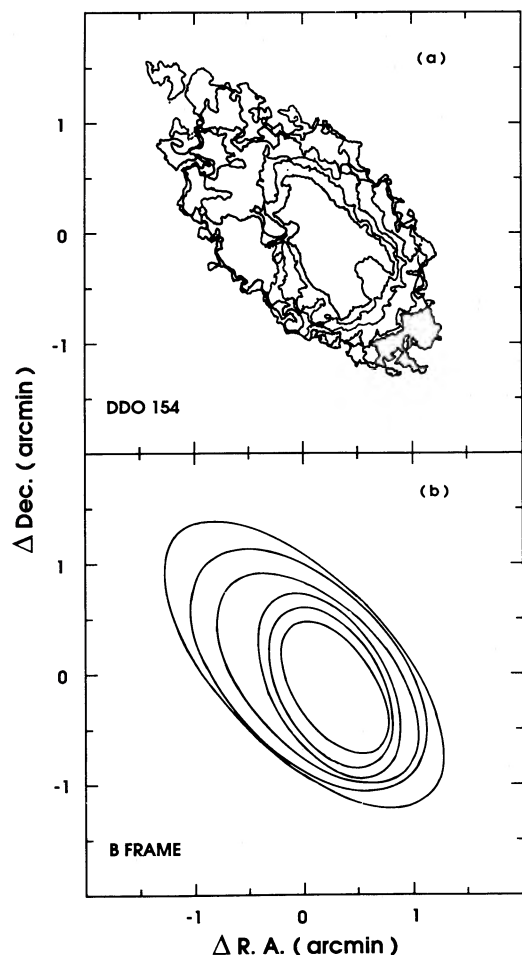


FIG. 3.—Optical isophotes (a) and fitted ellipses (b) in B for DDO 154 from 24.0 to 26.5 mag arcsec $^{-2}$ in steps of 0.5 mag.

the northeast. While the derived inclination of the galaxy for each isophote is fairly constant at $57^{\circ}.5$, the outermost isophote suggests a value $\sim 7^{\circ}$ – 8° larger. As for the position angle, we see clearly that there is a difference of $\approx 10^{\circ}$ between the inner and outer parts.

TABLE 2
ELLIPSE FITS TO THE ISOPHOTES OF DDO 154

μ_B (1)	X_c (2)	Y_c (3)	a (4)	b/a (5)	i (6)	θ (7)
24.0.....	-2.8	-0.9	40.3	0.54	59.6	33.4
24.5.....	-0.7	-1.0	47.1	0.59	55.9	29.5
25.0.....	0	0	54.5	0.57	57.4	30.2
25.5.....	6.0	3.8	68.5	0.56	58.1	43.3
26.0.....	11.2	8.4	79.0	0.57	57.4	43.8
26.5.....	13.8	11.4	97.6	0.47 ^a	64.8	44.1

^a Not used to calculate the mean inclination.

Col. (1).—Surface brightness of the isophotes in mag arcsec $^{-2}$.

Cols. (2) & (3).—Offset of the center of the isophotes in arcsec. East and north are positive.

Col. (4).—Major axis in arcsec.

Col. (5).—Ratio of minor to major axis.

Col. (6).—Inclination $i = \cos^{-1} [(q^2 - q_0^2)/(1 - q_0^2)]^{1/2}$, where $q = b/a$ and $q_0 = 0.22$ is the assumed intrinsic flattening (Bottinelli *et al.* 1983).

Col. (7).—Position angle of the major axis.

TABLE 3
LUMINOSITY PROFILES OF DDO 154

Radius (arcmin)	μ_B (mag arcsec $^{-2}$)	$(B-V)$	$(B-R)$
0.12.....	23.51	0.39	0.71
0.26.....	23.61	0.47	0.73
0.42.....	23.93	0.36	0.65
0.59.....	24.27	0.32	0.56
0.75.....	24.62	0.31	0.56
0.92.....	25.04	0.36	0.61
1.09.....	25.38	0.44	0.72
1.25.....	25.82	0.33	0.60
1.42.....	26.36	0.54 ^a	0.90 ^a
1.59.....	26.81	0.59 ^a	0.69
1.75.....	27.24	0.56 ^a	0.64
		$\langle 0.37 \rangle$	$\langle 0.64 \rangle$
		± 0.06	± 0.07

^a Not used to calculate the mean colors.

To calculate the elliptically averaged profile, we used the mean orientation parameters derived from the outer B isophotes ($25.0 \leq r \leq 26.0$) which are less perturbed by bright stars and H II regions. The B luminosity profile and the $(B-V)$ and $(B-R)$ colors are shown in Figure 4 and given in Table 3. It can be seen that despite the very irregular optical appearance, the luminosity profile is very regular and is almost a pure exponential for $0.25 \leq r \leq 1.75$. The regularity of the profile is partly due to the fact that the data were averaged in ellipses.

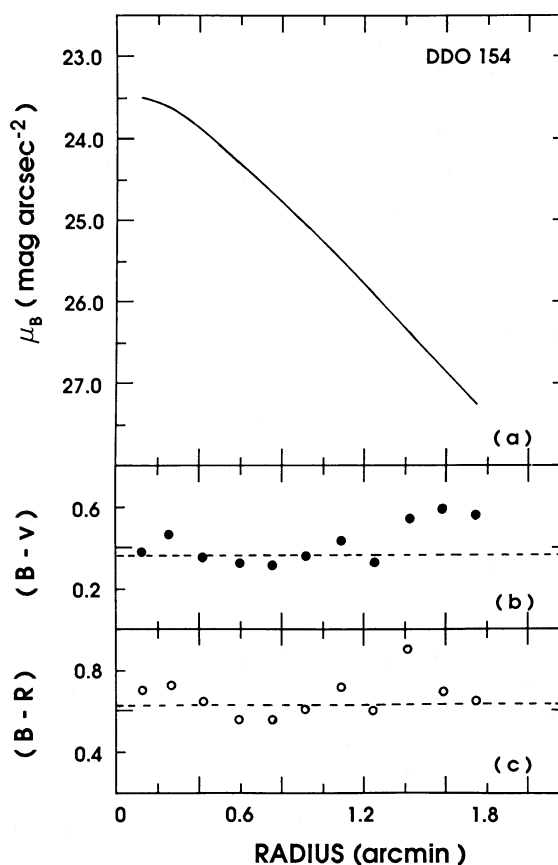


FIG. 4.—Luminosity profile in B (a) and radial color distribution $(B-V)$ (b) and $(B-R)$ (c) for DDO 154.

This will tend to smear out local irregularities such as OB associations which can contribute significantly to the light but not much to the mass. A cut along the major axis or a pie-shape profile would show much more structure. However, those features are not dynamically significant. What is needed is the distribution of the underlying light and hence of the luminous mass distribution. The flattening in the very inner parts ($r < 0.25$) could be due to internal absorption. This profile is similar to what is seen in more luminous irregulars (see, e.g., NGC 3109; Carignan 1985). The colors, fairly constant around $(B - V) = 0.37$ and $(V - R) = 0.27$, are typical of Im galaxies when compared with synthetic colors (Carignan 1983) computed using Coleman, Wu, and Weedman (1980) spectral energy distribution [$(B - V) = 0.32$, $(V - R) = 0.30$].

An exponential fit to the B luminosity profile ($r > 0.25$) yields an extrapolated central surface brightness of 22.76 which, when corrected for galactic extinction and line-of-sight integration, gives $B(0)_c = 23.17$. Both those corrections are somewhat uncertain and should be considered as upper limits. This translates in a possible range for $B(0)_c$ from 22.74 to 23.17. This low surface brightness is comparable to the nearby Magellanic-type spiral NGC 3109 (Carignan 1985). For the exponential scale length, we find $\alpha^{-1} = 0.43$ in B , 0.47 in V , and 0.44 in R . For this study, the B value $\alpha^{-1} = 0.50$ kpc is adopted.

Finally, integrating the luminosity profile, we get a total apparent magnitude of $B_T = 14.39$ which, when corrected for galactic extinction gives $B_T^0 = 14.20$. Because, in the case of DDO 154 the amount of internal absorption is too uncertain, no attempt was made to correct for it. So, this value should be considered as a lower limit. At our adopted distance of 4 Mpc, this implies an absolute magnitude of -13.81 which corresponds to a total blue luminosity of $5.0 \times 10^7 L_{B\odot}$. The photometric parameters are summarized in Table 4.

TABLE 4
OPTICAL PARAMETERS OF DDO 154 (NGC 4789A)

Parameter	Value
R.A. (1950) ^a	12 ^h 51 ^m 39 ^s .6
Decl. (1950) ^a	+27° 25' 30"
Type ^a	IB(s)m IV-V
Distance (Mpc) ^b	4.0
Mean axis ratio ($0.2 \leq r \leq 1.8$)	0.57 ± 0.02
Inclination ($q_0 = 0.22$)	57.4 ± 1.5
Position angle (1986.1):	
(inner parts: $0.2 \leq r \leq 0.8$)	32.6 ± 2.1
(outer parts: $1.2 \leq r \leq 1.8$)	43.2 ± 2.2
Parameters at $\mu_B = 25.0$ mag arcsec ⁻² :	
Major axis	$D_{25} = 1'.8$
Minor axis	$d_{25} = 1'.1$
Holmberg radius ($\mu_B = 26.6$ mag arcsec ⁻²)	$R_{Ho} = 1'.5$
Exponential disk parameters:	
Corrected central surface brightness ^{c,d}	$B(0)_c = 23.17^{+0.15}_{-0.45}$
Scale length (kpc)	$\alpha^{-1} = 0.50 \pm 0.05$
Total apparent magnitude	$B_T = 14.39 \pm 0.05$
Corrected apparent magnitude ^{d,e}	$B_T^0 = 14.20$
Corrected absolute magnitude	$M_T^0(B) = -13.81$
Total blue luminosity ^f	$L_T(B) = 5.0 \times 10^7 L_{B\odot}$

^a de Vaucouleurs *et al.* 1976 (RC2).

^b Adopted for this study (§ III).

^c Line-of-sight integration correction = $2.5 \log R_{25} = 0.60$.

^d Galactic extinction $A_B = 0.19$ (RC2).

^e No correction for internal absorption.

^f In solar units, with $M_{B\odot} = +5.43$.

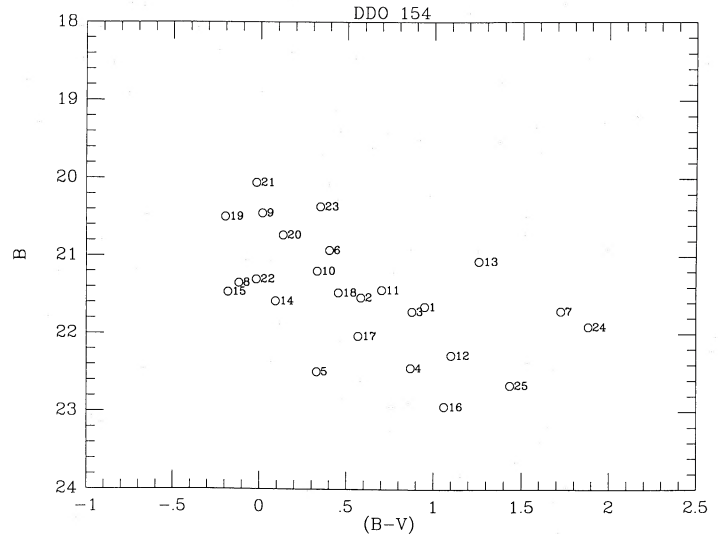


FIG. 5.—Color-magnitude B vs. $(B - V)$ diagram for the stars listed in Table 5. Those 25 stars were observed in all four filters. Stars 21, 9, and 19 were used to estimate the distance modulus.

b) Photometry of the Brightest Blue Stars

As can be seen on Figure 1, the brightest stars of DDO 154 are well resolved. At such a high galactic latitude ($b = 89.4^\circ$), the chance superposition of galactic foreground stars is minimal. We thus decided to obtain the photometry of the brightest blue stars. The brightest red stars were not used since no information is available on their possible variability. The photometry was done using DAOPHOT (Stetson 1987). Twenty-five stars were found in all filters and used for the analysis. Figure 5 shows the resulting $C - M$ diagram and the results for each star are given in Table 5.

TABLE 5
PHOTOMETRY OF THE RESOLVED STARS IN DDO 154

Star No.	X	Y	B	$(B - V)$	$(V - R)$	$(R - I)$
1.....	80.6	301.4	21.66	0.95	0.57	0.77
2.....	95.5	258.8	21.54	0.58	0.31	0.49
3.....	98.5	251.2	21.72	0.87	-0.14	1.46
4.....	99.6	361.9	22.44	0.87	0.62	0.91
5.....	107.3	348.5	22.49	0.33	0.79	0.95
6.....	110.9	212.7	20.94	0.40	0.24	0.52
7.....	111.3	372.4	21.71	1.72	0.59	0.91
8.....	119.3	265.4	21.35	-0.12	0.26	0.19
9.....	122.2	283.0	20.46	0.01	-0.05	0.42
10.....	126.4	270.7	21.20	0.33	0.07	-0.10
11.....	132.2	262.0	21.44	0.70	-0.06	0.69
12.....	135.6	259.6	22.28	1.10	0.83	0.59
13.....	139.4	213.2	21.07	1.26	-0.12	1.28
14.....	151.6	291.5	21.59	0.09	0.53	0.40
15.....	153.2	250.8	21.47	-0.18	0.13	0.81
16.....	156.5	193.2	22.94	1.06	0.36	1.17
17.....	159.4	288.9	22.04	0.57	0.31	-0.05
18.....	161.4	283.3	21.48	0.45	-0.00	0.08
19.....	174.6	268.3	20.50	-0.20	0.02	0.34
20.....	183.0	216.5	20.74	0.13	0.13	0.71
21.....	185.6	263.3	20.06	-0.02	0.07	-0.06
22.....	191.9	285.4	21.31	-0.02	0.09	0.11
23.....	199.3	245.9	20.37	0.35	0.35	0.30
24.....	208.9	196.7	21.91	1.88	0.31	0.56
25.....	221.8	166.2	22.66	1.43	0.07	0.96

Two different calibrations are available to estimate the distance modulus. Because of the well-known dependence between the absolute magnitude of the brightest blue stars and the absolute magnitude of the parent galaxy, only the data on Sextan A, Sextan B, and WLM (Sandage and Carlson 1985a, b), which are systems comparable to DDO 154 [$M_T(B) = -14.3, -14.3,$ and $-13.5,$ respectively] will be used. The other calibration is the one given by de Vaucouleurs (1978).

From the photometry, we get $(B_1^*) = 20.06$ [$(B-V) = -0.02$] for the brightest blue star (No. 21) and $\langle B(3) \rangle = 20.34 \pm 0.24$ [$\langle (B-V) \rangle = -0.07 \pm 0.11$] for the mean apparent magnitude of the three brightest blue stars (No. 21, No. 9, No. 19). If star No. 23 was used instead of star No. 19, the mean would only change by 0.04 mag. Using the mean absolute magnitude in Sextan A, Sextan B, and WLM of $\langle M_B(3) \rangle = -7.15 \pm 0.40$ a distance of 3.2 ± 0.9 Mpc is derived. On the other hand, using de Vaucouleurs (1978: relations 4 and 5b) and correcting our total magnitude for internal absorption [$A(i) = 0.8 \log R_{25} = 0.19$] a distance of 3.2 ± 1.0 Mpc is also derived.

One ought to be careful, however, because of the well-known problems with this technique; namely, the possible contamination by foreground stars and the possibility that the brightest blue stars could in fact be compact clusters (Moffat, Seggewiss, and Shara 1985). In both cases, this would lead to an underestimate of the distance modulus. Nevertheless, we think that the brightest star method is still valuable if used in conjunction with other distance indicators.

c) Adopted Distance

From its position on the sky, de Vaucouleurs (1975) suggested that DDO 154 could be associated with either the nearby Canes Venaticorum I cloud at 3.8 Mpc or the more distant Coma I cloud at 9.6 Mpc. In a previous paper (Carignan and Freeman 1988), we favored the small distance based on the qualitative argument that the brightest stars could easily be resolved. This is now substantiated by the quantitative study just presented which suggests that even the small distance is probably an upper limit.

Moreover, DDO 154's radial velocity of 375 km s^{-1} also suggests that the galaxy is more likely to be associated with the CVn I cloud which has a mean velocity of 342 km s^{-1} (range: 256–530). This can be compared with the two subgroups of the Coma I cloud where we find a mean velocity of 829 km s^{-1} (range: 622–1078) for the NGC 4274 group and 1134 km s^{-1} (range: 876–1305) for the NGC 4565 group.

Based on both the magnitudes of the brightest blue stars and the more likely association with the CVn I cloud, we favor a distance of 4 Mpc over 10 Mpc (Krumm and Burstein 1984) as would be obtained using the Tully-Fisher relation (Tully and Fisher 1977: TFR). The reasons for such a discrepancy using the TFR are discussed in the last section. Because the H I mass, which is dynamically more important than the stellar disk (see § V), scales as the square of the distance, it is important to be able to decide between those two possibilities.

IV. 21 cm STUDIES

The CLEANed channel maps at $45''$ resolution are shown in Figure 6. The rms noise in those maps is 1.3 mJy per beam. Already in those maps, a warp of the H I disk is clearly visible in the outer parts (see i.e. the channels at 416.2 and 333.8 km s^{-1}).

a) Global H I Properties

The global H I profile for DDO 154 is given in Figure 7. From it, a midpoint velocity of $375 \pm 2 \text{ km s}^{-1}$ is found which is similar to Krumm and Burstein's (1984) value and almost identical to the systemic velocity of $374 \pm 2 \text{ km s}^{-1}$ given by Allen and Shostak (1979). However, our flux integral of $72 \pm 10 \text{ Jy km s}^{-1}$ is smaller than what was obtained in those two studies (106 ± 5 and $94 \pm 7 \text{ Jy km s}^{-1}$, respectively) which seems to indicate that we have been missing flux with our VLA observations. Such a discrepancy between the VLA flux and single dish fluxes is not uncommon. Recently, it was seen for another dwarf irregular, Sextan A (Skillman *et al.* 1988), where it was identified with a low-density, very extended component. Our derived value of $2.7 \times 10^8 M_\odot$ for the total H I mass ($\Delta = 4$ Mpc) and 5.4 for the H I mass-to-light ratio are thus lower limits. Nevertheless, with $(M_H/L_B) = 5.4$, DDO 154 is the most gas-rich galaxy in the Nearby Galaxies Catalog (Tully 1988) and is comparable to the low surface brightness more massive system Malin 1 which was $(M_H/L_B) \approx 5$ (Bothun *et al.* 1987).

The total H I map obtained by the moment analysis was already shown elsewhere (Carignan and Freeman 1988). In Figure 8, a straight sum of the 13 channels with H I emission is shown. While not going as deep as the map derived by the moment analysis, it still shows very clearly the warp of the H I disk, especially on the SW side. The H I distribution is regular and extends to $\approx 5 D_{H_0}$ at a level of $1 \times 10^{19} \text{ cm}^{-2}$. The level of $1 \times 10^{21} \text{ cm}^{-2}$, considered as a critical surface density for massive star formation and determined by observations of nearby irregular galaxies (Skillman 1987), corresponds almost exactly to the Holmberg diameter.

Figure 9 gives the radial distribution of H I surface densities. Contrary to most spirals (Sancisi 1988) and other irregulars (Skillman *et al.* 1987), there is very little flattening of the H I distribution in the inner regions. This is to be expected in such a system where so little gas has been processed into stars and it is consistent with the fact that no molecular gas has been detected. For $r > R_{H_0}$, the H I follows almost exactly an exponential law with a scale length of $1/4$ (1.65 kpc). This exponential decrease is compatible with the much larger extent of the H I disk as compared to the stellar component.

b) H I Kinematics

The velocity field derived by the moment analysis of the $60''$ resolution data is shown in Figure 10 (Plate 11). We see that far from being chaotic, the isovelocity contours are regular and well-defined. At this stage, it is too early to know if the closing of the outermost contours means that the rotation curve is really decreasing or if it is due to the warp seen in the H I distribution. A Gaussian profile fitting technique was also used to derive the velocity field. Both this technique and the moment analysis yield essentially similar results. For the rest of the analysis, the results from the moment analysis will be used. To illustrate that the velocity field is a good representation of the data, we have superposed in Figure 11 a cut of the velocity field onto an $L-V$ (position-velocity) diagram, both taken along the major axis.

To derive the rotation curve, the $45''$ resolution data were used. The method is described in Carignan, Sancisi, and van Albada (1988), and van Albada *et al.* (1985). After dividing the velocity data into $30''$ concentric annuli in the plane of the galaxy, a least-squares solution is found for the five kinematical parameters (the rotation center $[x_0, y_0]$, the systemic

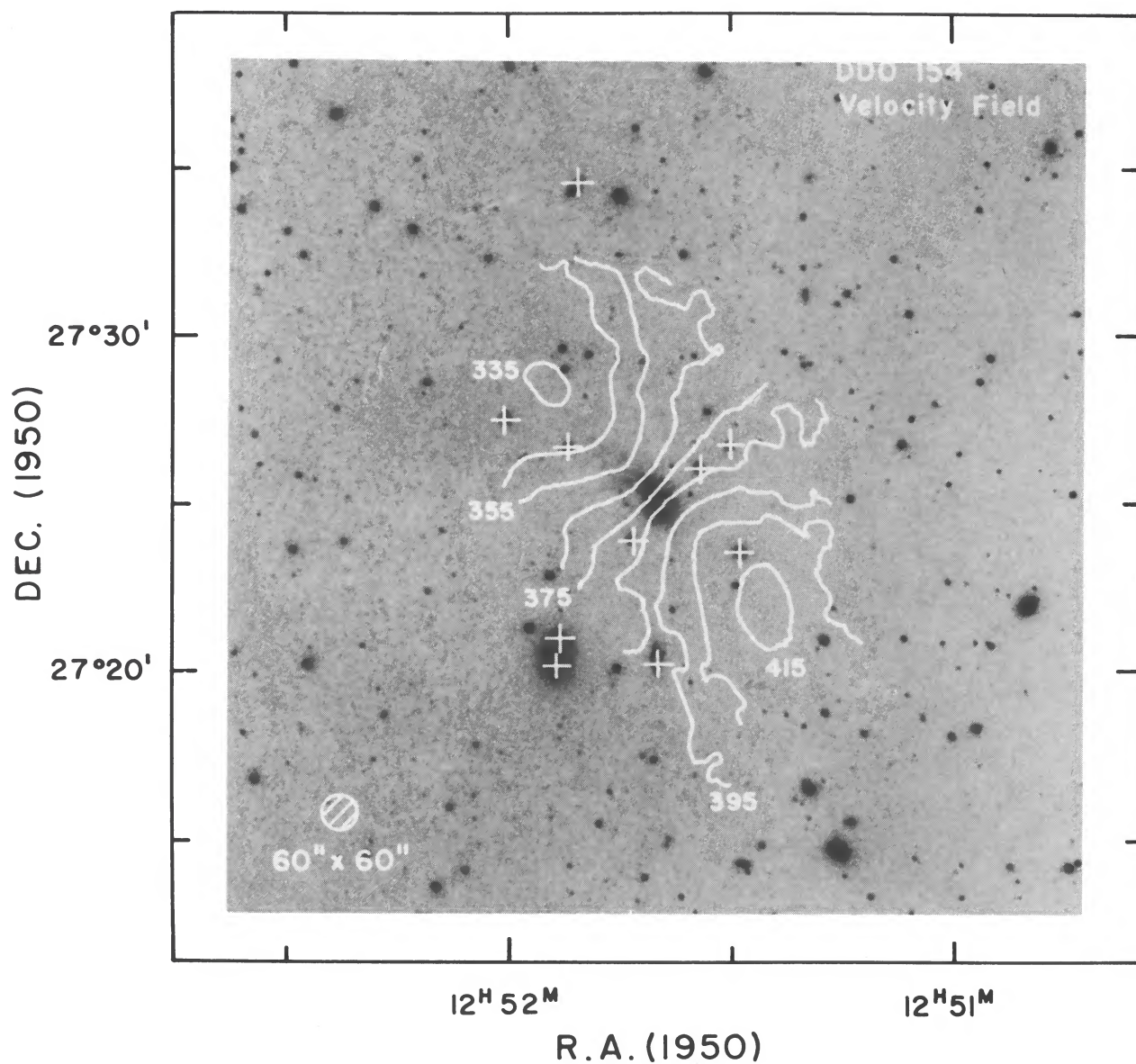


FIG. 10.—Isovelocity contours for DDO 154, superposed on an optical photograph using the 60" resolution data (see bottom left). The contour interval is 10 km s⁻¹ from 335 to 415 km s⁻¹ heliocentric radial velocities.

CARIGNAN AND BEAULIEU (see 347, 764)

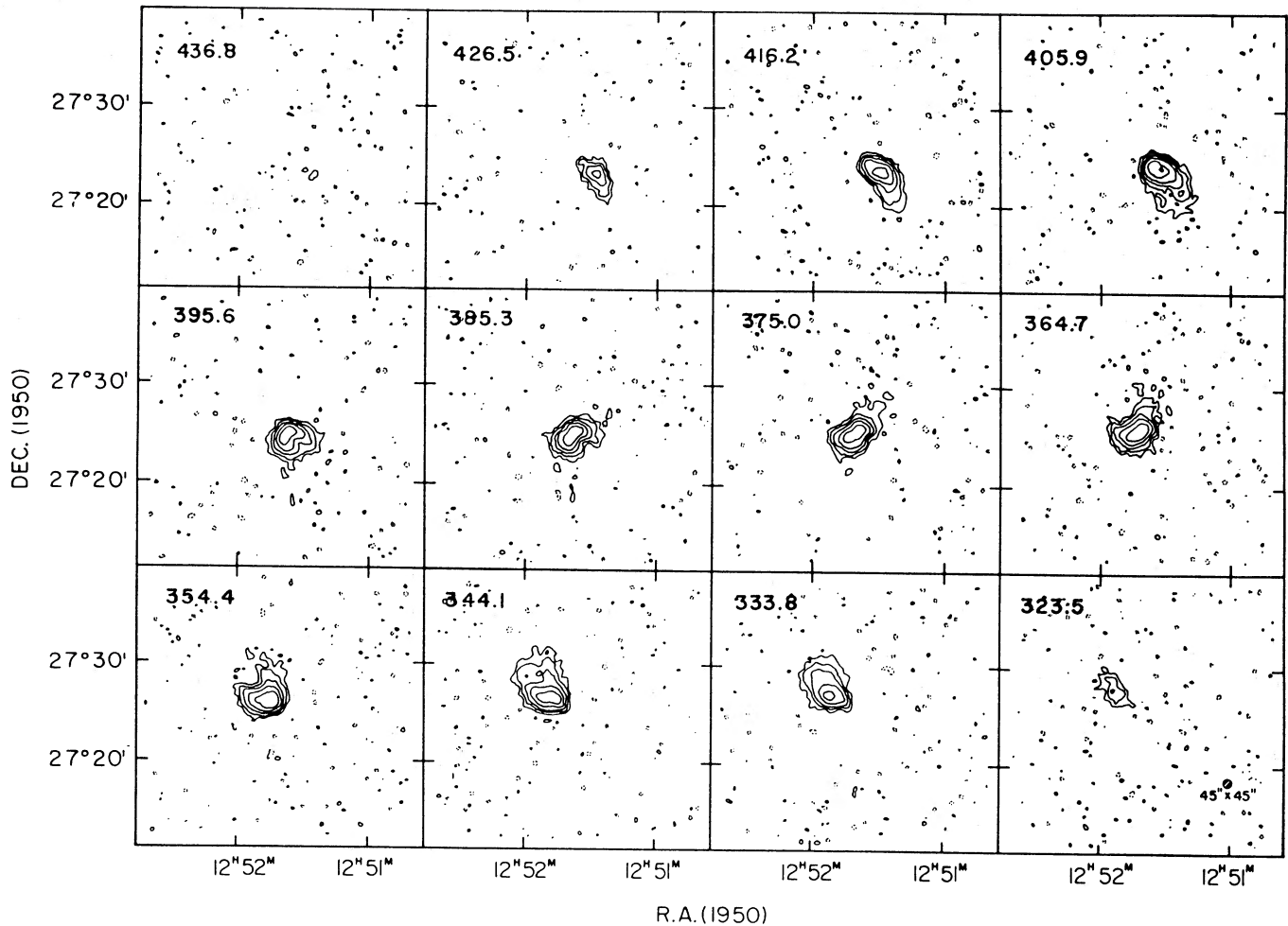


FIG. 6.—H I line channel maps after smoothing the original data (resolution = $33''.5 \times 35''.3$) to a circular Gaussian beam of $45''$ (see bottom right-hand corner). The channel separation is 10.31 km s^{-1} . The heliocentric radial velocities (km s^{-1}) of each channel are indicated in the upper left-hand corner. These maps show the distribution of H I brightness temperature in each velocity channel. The contours are $-1, 1 (2.5 \sigma), 2, 4, 8, 16 \text{ K}$. The negative contours are dashed and the zero-level contour is omitted. The maps are not corrected for primary beam (HPBW = $32''$) attenuation.

velocity V_{sys} , the inclination i , and the position angle θ that best represent the velocity field at each radius. In this way, any warp of the H I disk is clearly seen through variations of i and θ with radius.

The analysis was done in two steps. First, using only the data in the inner parts (excluding the warped region), and keeping i and θ fixed (using the optical values), we looked for the rotation center and the systemic velocity. We found that the rotation center coincides with the optical center and that the systemic velocity is $375 \pm 2 \text{ km s}^{-1}$, similar to the value derived from the global profile. Then, keeping those parameters fixed, we let i and θ vary at all radii. The final kinematical solution for the whole galaxy is illustrated in Figure 12 along with separate solutions for the approaching and receding sides.

From Figures 12a and b, it can be seen that for $r \leq 4.5$ the inclination and position angle are nearly constant at $i \approx 64^\circ$ and $\theta \approx 46^\circ$. Those values are very close to the ones found for the last optical isophote. For $r \geq 5.0$, the presence of the warp is clearly seen: the galaxy becomes more face-on ($i \approx 60^\circ$), and the position angle gets smaller. As already visible in the total H I map, this change in position angle is more clearly seen on the southwest than on the northeast side. In fact, there is not

enough H I on the northeast side to find a solution for the inclination and position angle at the last point.

In Figure 12c, we see that the global rotation curve is a good representation of both sides of the galaxy. The mean difference between the southwest and northeast velocities is $\langle \Delta V_{\text{rot}} \rangle < 1.0 \text{ km s}^{-1}$, the biggest difference being 1.8 km s^{-1} at $r = 5'$. The adopted rotation curve is given in Table 6. It can be compared with the one given in Carignan and Freeman (1988) using the velocity field derived by a Gaussian analysis. The differences are everywhere less than 3 km s^{-1} . Corrections for the asymmetric drift have been calculated and found negligible at all radii.

c) Rotation Curve Analysis

The first striking feature about this rotation curve is that we have clearly reached the flattening part, while all other rotation curves derived so far for dwarf irregulars continue to rise at the last measured point (Tully *et al.* 1978; Skillman *et al.* 1987). Moreover, there is a clear suggestion that the rotation curve may be declining at large radii. It thus seems that the closing of the isovelocity contours mentioned earlier cannot all be accounted for by the warp of the H I disk.

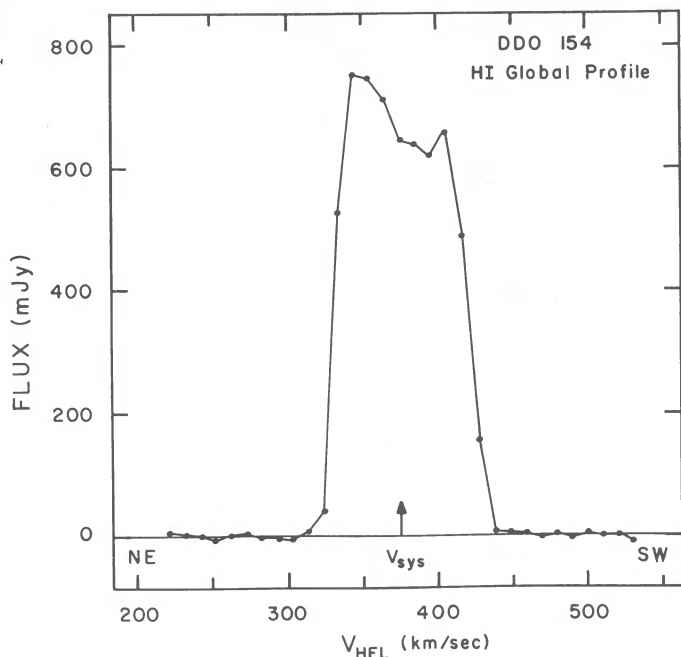


FIG. 7.—H I global profile for DDO 154 obtained by integrating the individual channel maps over the area of the source after subtraction of the continuum background. The channel spacing is 10.31 km s^{-1} . Integration of the profile gives a total flux of 72 Jy km s^{-1} .

If the decline of the rotation curve is real, *DDO 154* could be one of the first systems where the edge of the mass distribution has been reached. However, one has to realize that this is based on the last three points of the rotation curve and that only two points are independent. Moreover, the difference between the

TABLE 6
ROTATION CURVE OF DDO 154

Radius (arcsec)	V_{rot} (km s^{-1})	Error (km s^{-1})
30.....	13.8	± 1.6
60.....	21.6	± 0.8
90.....	28.9	± 0.7
120.....	34.3	± 0.5
150.....	38.2	± 0.4
180.....	42.0	± 0.2
210.....	44.6	± 0.2
240.....	46.3	± 0.2
270.....	47.4	± 0.3
300.....	48.2	± 0.6
330.....	47.4	± 0.7
360.....	45.5	± 1.3
390.....	43.1	± 2.0

last point and the maximum velocity V_{max} is only at a 2.5σ level.

While the least-squares analysis cannot find a solution for $r > 6.5$, it can be seen in Figure 8 that there is low-level H I emission out to $r \sim 8'$. In order to get information on the orientation parameters in those outer parts, we used the data smoothed at $60''$ and fitted ellipses to the H I isophotes. The results, compared with the least-squares solution, are given in Figure 13. The differences are everywhere less than or equal to 2.5 km s^{-1} . There are now three independent points confirming the trend that the rotation curve is declining and the difference between the last point and V_{max} has reached 7 km s^{-1} . With this result, we can be more confident that we are really seeing the declining part of the rotation curve and that probably most of the mass (luminous and nonluminous) is within 9 kpc from the center.

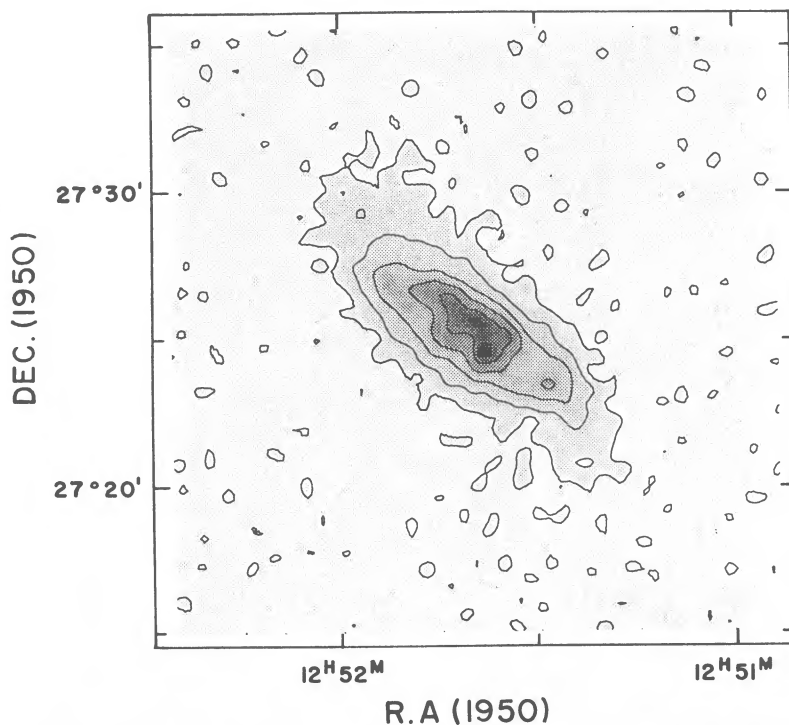


FIG. 8.—Sum of the 13 channels with line emission at $45''$ resolution. The contours correspond to H I surface densities of $0.6, 2.5, 5.9, 9.3,$ and $12.7 \times 10^{20} \text{ cm}^{-2}$. The map is not corrected for primary beam attenuation.

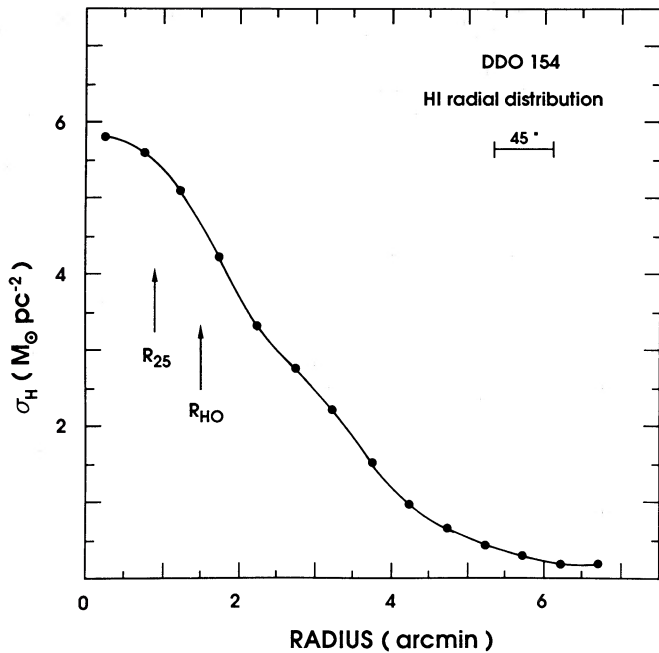


FIG. 9.—H I radial distribution obtained by averaging the surface densities of the moment analysis total H I map in circular annuli in the plane of the galaxy. The parameters used for the deprojection are P.A. = 46°5 and $i = 64^\circ$.

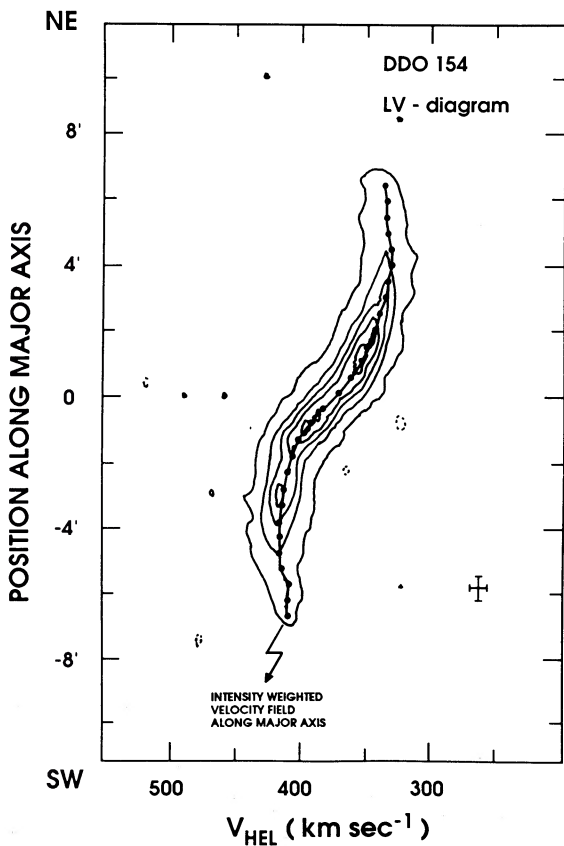


FIG. 11

FIG. 11.—Cut of the intensity weighted velocity field superposed on a position-velocity plot ($L-V$ diagram). The contours are $-3, 3, 23$ to 83 mJy per beam in steps of 20 . Negative contours are dashed and the zero contour is omitted.

FIG. 12.—Least-squares solution for i (a), θ (b), and V_{ROT} (c) derived from the analysis of the velocity field at $45''$ resolution. A global solution (squares) and separate solutions for the approaching and receding sides are shown.

V. MASS DISTRIBUTION

The models used to study the mass distribution are described in Carignan (1985) and Carignan and Freeman (1985). To calculate the mass distribution of the stellar disk, the B luminosity profile (§ III) is used with the assumption of constant $(M/L_B)_*$. An intrinsic flattening of $q_0 \equiv c/a = 0.22$ (Bottinelli *et al.* 1983) is assumed for the stellar disk. For the H I component, we take the H I surface densities of Figure 9. It is assumed that the H I layer is infinitely thin. Molecular hydrogen H_2 would also be included in the luminous component, if it had been detected. For the dark halo component, an isothermal sphere model is used. The isothermal sphere can be described by two parameters: the core radius r_c and the one-dimensional velocity dispersion σ . The central density is then given by $\rho_0 = 9 \sigma^2 / 4\pi G r_c^2$. A first analysis of the dark content of DDO 154 was given in Carignan and Freeman (1988). In this paper, we analyze the mass distribution in more detail.

a) Two-Component (Luminous and Dark) Model

In order to be able to represent the rotation curve over the whole radius range, a dark isothermal halo was added to the luminous component (stars and H I). The best-fitting model is shown in Figure 14b. The halo has a core radius $r_c = 3.0$ kpc

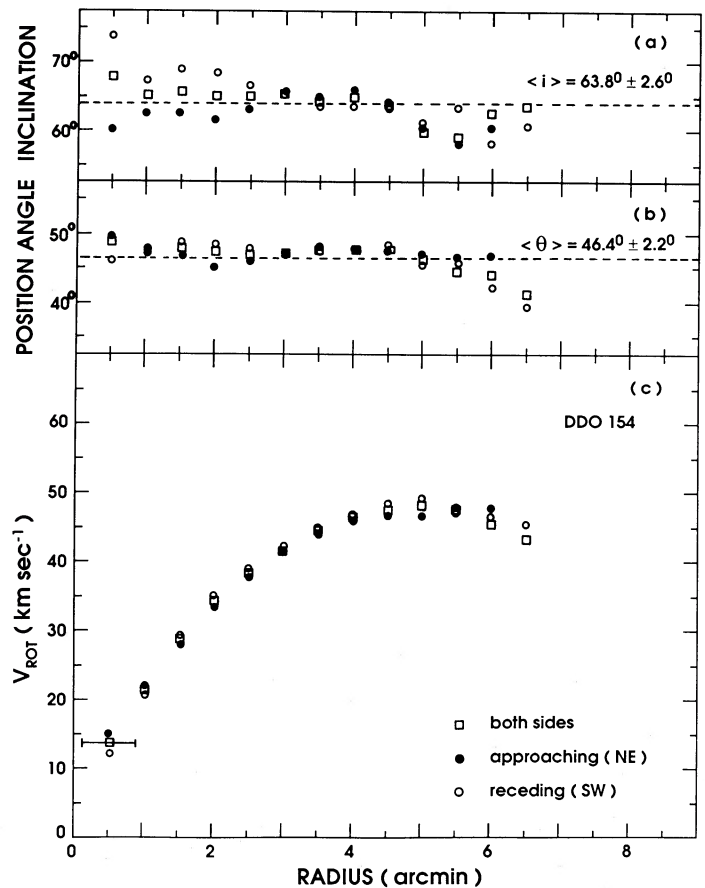


FIG. 12

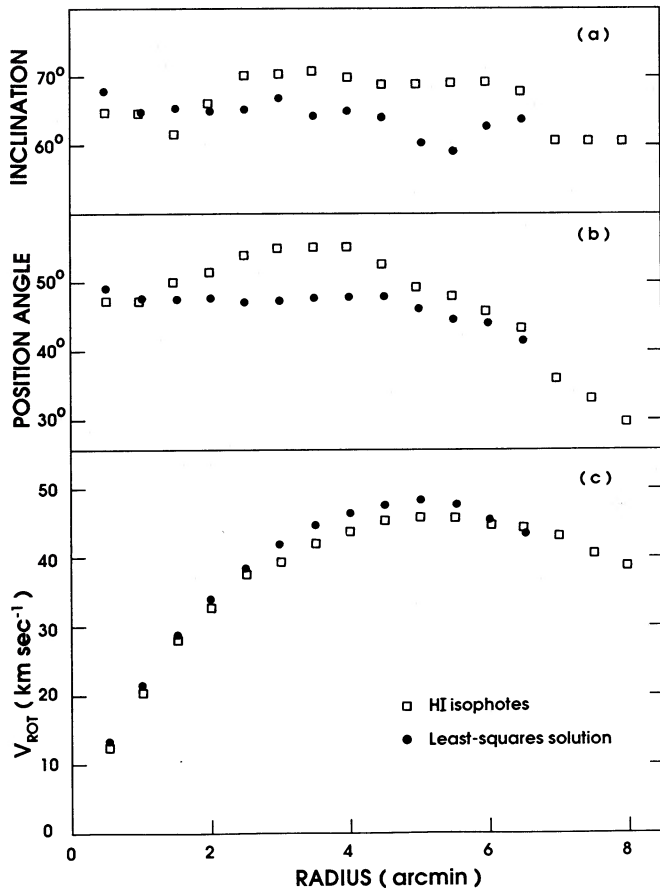


FIG. 13.—The inclination (a), position angle (b), and V_{ROT} (c) derived by fitting the H I isophotes (squares) are compared to the least-squares solution (circles) shown in Fig. 11.

and a one-dimensional velocity dispersion $\sigma = 28 \text{ km s}^{-1}$. This corresponds to a central density of $\rho_0 = 0.015 M_{\odot} \text{ pc}^{-3}$. The small differences (1 km s^{-1} in σ which translates into $0.001 M_{\odot} \text{ pc}^{-3}$ in ρ_0) between this model and the one in Carignan and Freeman (1988) come from the fact that we used the rotation curve derived by a moment analysis while they used the rotation curve obtained by a Gaussian profile analysis. Multiplying the H I component by 4/3 to include a correction for the He content brings no change to the parameters of the best-fitting halo.

For the stellar disk, we get $(M/L_B)_* = 1.0 (M_{\odot}/L_{\odot})$: smaller values underestimate V_{ROT} for $r < 2 \text{ kpc}$, and larger values overestimate V_{ROT} for $1 < r < 3 \text{ kpc}$. In any case, the exact value of the disk mass-to-light ratio is not critical since the rotation curve is completely dominated by the dark component for $r > 2 \text{ kpc}$. Moreover, because of the well-defined turnover of the rotation curve for $r > 5 \text{ kpc}$, there is no ambiguity on the maximum velocity of the halo as in the case of "solid-body" type rotation curve (Tully *et al.* 1978; Skillman *et al.* 1987). Because of those two factors, it is possible to constrain almost uniquely the parameters of the mass model.

At the last measured point ($r = 7.6 \text{ kpc}$), the model has a total mass (luminous and dark) of $3.8 \times 10^9 M_{\odot}$ of which more than 90% is dark. This gives a $(M/L_B)_{\text{total}} > 75$. As for the luminous component, we get $5.0 \times 10^7 M_{\odot}$ for the stellar disk and $2.7 \times 10^8 M_{\odot}$ for the H I component. This means that there is 5 times more mass in H I than in stars.

b) Dark Matter Distribution

The model of Figure 14b, while giving a reasonable fit to the observed rotation curve, assumes a functional form (isothermal halo) for the distribution of the dark material. While this form is convenient to use and justified by its asymptotic density distribution, it has been shown (Blumenthal *et al.* 1986) that while the dark halos may have started with an isothermal density distribution they most likely do not have such a distribution at the present epoch.

Figure 14a shows the local ratio of the total mass to (1) the stellar disk mass M_* and (2) the H I gas mass M_{HI} . As we get to greater radii, the total mass is almost all dark mass. It is interesting to notice that while the total mass is not at all distributed like the stars, its ratio to the H I mass is much flatter. To illustrate this similarity, Figure 15 shows a model where the H I mass has been scaled by a factor of 7. We see that it represents the rotation curve very well out to 5 kpc, the difference being less than or equal to 6 km s^{-1} out to the last measured point.

We do not expect such a model to represent perfectly the rotation curve since we know that the distribution of the H I gas is probably much flatter than the distribution of the dark material. However, if the missing flux in the VLA observations is mainly in large-scale low surface brightness structures in the outer parts, as we expect, the discrepancy could be even smaller. The similarity between the way the total mass (and in this case the dark mass) and the H I gas are distributed is not peculiar to this dwarf system but is also seen in large spirals like NGC 6946 (Carignan *et al.* 1989) at $M_B = -21.5$. This fact was also noted previously by Bosma (1978) and Sancisi (1983).

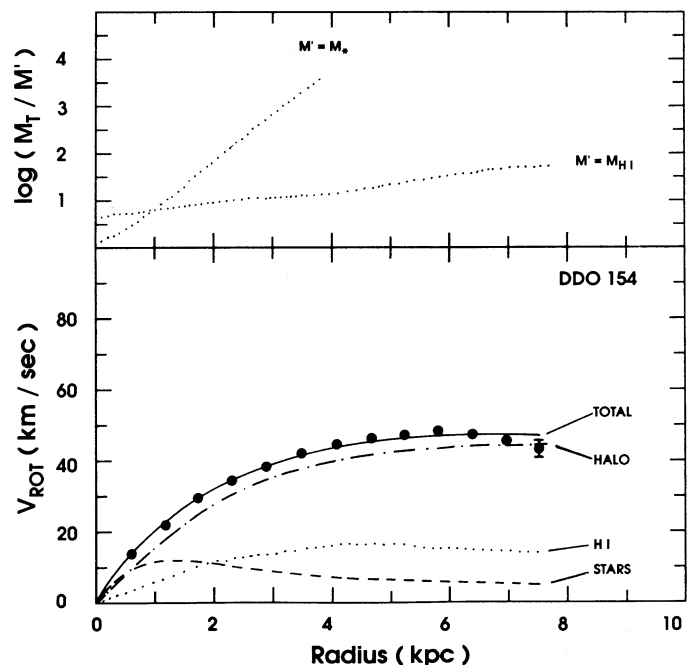


FIG. 14.—(a) Ratio of the local total (luminous and dark) mass to the stellar mass M_* and to the H I mass M_{HI} . (b) Complete mass model for DDO 154 using the rotation curve of Table 5. When not indicated, the errors are smaller than the size of the symbols. The contribution of the H I component was calculated using the surface densities of Fig. 9. The total H I mass is $2.7 \times 10^8 M_{\odot}$. The stellar disk has $(M/L_B)_* = 1.0$, giving a total mass of $5.0 \times 10^7 M_{\odot}$. The halo parameters are $r_c = 3.0 \text{ kpc}$ and $\rho_0 = 0.015 M_{\odot} \text{ pc}^{-3}$. The total mass (dark and luminous) at the last observed velocity point (7.6 kpc) is $3.8 \times 10^9 M_{\odot}$.

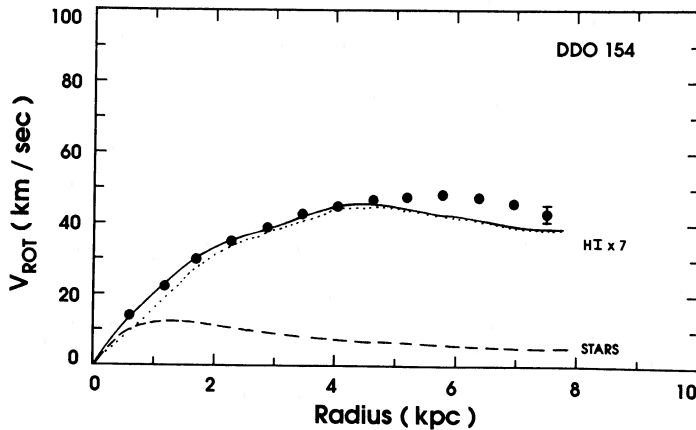


FIG. 15.—Mass model for DDO 154 where the H I surface densities have been multiplied by a factor of 7_{\odot} ($M/L_B)_* = 1$ for the stellar disk.

It is just seen much better in the case of DDO 154 because the H I is so extended.

VI. SUMMARY AND CONCLUSIONS

An optical and H I study of the gas-rich dwarf irregular galaxy DDO 154 has been presented. The main results from the optical observations are the following.

1. Despite the chaotic appearance, the orientation parameters of the isophotes are well determined. A mean inclination of 57.4° is found. As for the position angle, it varies from $\sim 33^\circ$ in the inner parts ($r < 1'$) to $\sim 43^\circ$ in the outer parts.

2. The luminosity profile is well defined and almost a pure exponential for $r > 0.25$. The flattening for $r < 0.25$ could be due to internal absorption. The exponential fit gives a very low extrapolated central surface brightness of $B(0)_c = 23.17$ and a scale length of 0.50 kpc.

3. The mean colors of $(B - V) = 0.37$ and $(V - R) = 0.27$ are typical for Im galaxies.

4. The photometry of the brightest blue stars suggests a distance of 3.2 ± 1.0 Mpc. Combined with the likely association of DDO 154 with the Cn V I cloud, a distance of 4 Mpc is adopted.

From the 21 cm H I line observations, the main results are as follows.

1. Using the global profile, a systemic velocity of 375 km s^{-1} and an integral flux of 72 Jy km s^{-1} are found. At the adopted distance, this flux translates into an H I mass of $2.7 \times 10^8 M_{\odot}$. With $M_{\text{HI}}/L_B \geq 5.4$, DDO 154 is thus one of the most gas-rich systems known.

2. The H I is very extended and reaches $\approx 5 D_{\text{H}_0}$ at a level of $1 \times 10^{19} \text{ cm}^{-2}$. A warp of the H I plane is clearly seen in the outer parts mainly on the SW side. Fitting an exponential to the outer parts of the H I distribution, we find a scale length of 1/4, more than 3 times that of the light distribution.

3. The velocity field is very regular. The kinematical solution gives fairly constant parameters of $i \approx 64^\circ$ and $\theta \approx 46^\circ$ out to $r = 4.5$. For $r > 5'$, the warp of the H I plane causes the inclination to become more face-on and the position angle to get smaller.

4. The rotation curve is unambiguously defined out to $4 R_{\text{H}_0}$ with very small differences between both sides of the galaxy. There is a clear flattening of the rotation curve for $r > 4'$ and even an indication that the declining part has been reached.

Combining both sets of data, a study of the mass distribution yields the following results:

1. In the case of this gas-rich system, the H I is dynamically more important than the stellar disk.

2. In order to reproduce the observed rotation curve, a dark isothermal halo with a core radius $r_c = 3.0$ kpc and a central density of $\rho_0 = 0.015 M_{\odot} \text{ pc}^{-3}$ was added to the luminous (stars and gas) component.

3. The best-fitting model gives $(M/L_B)_* = 1.0$ for the stellar disk. However, the parameters of the dark halo component are quite insensitive to the exact value of $(M/L_B)_*$ since it completely dominates the rotation curve for $r > 2$ kpc. At the last measured velocity point, more than 90% of the mass ($3.8 \times 10^9 M_{\odot}$) is dark.

4. Finally, we find that there is a very close relation between the way the total mass (and in this case the dark mass) and the H I mass are distributed.

One of the most important outcomes from this analysis is that the parameters of the mass model, and hence of the dark halo, are very well constrained. In less gas-rich and/or less extended systems, where only the "solid body" part of the rotation curve is seen, those parameters are often very uncertain because the maximum velocity of the halo component is not known. Another advantage of this system is that because a large fraction of the luminous mass (stars and gas) is in H I, this reduces the uncertainty coming from the $(M/L_B)_*$ value assumed for the stellar disk.

In Carignan and Freeman (1988), some differences between dwarfs and more massive galaxies were pointed out. It was suggested that the dark halos of dwarf galaxies are less massive, have higher central densities, and are smaller in radii. The results from this study suggest another important difference: namely, that the TFR may be breaking down at the low-mass end. Figure 16 shows a diagram M versus ΔV for

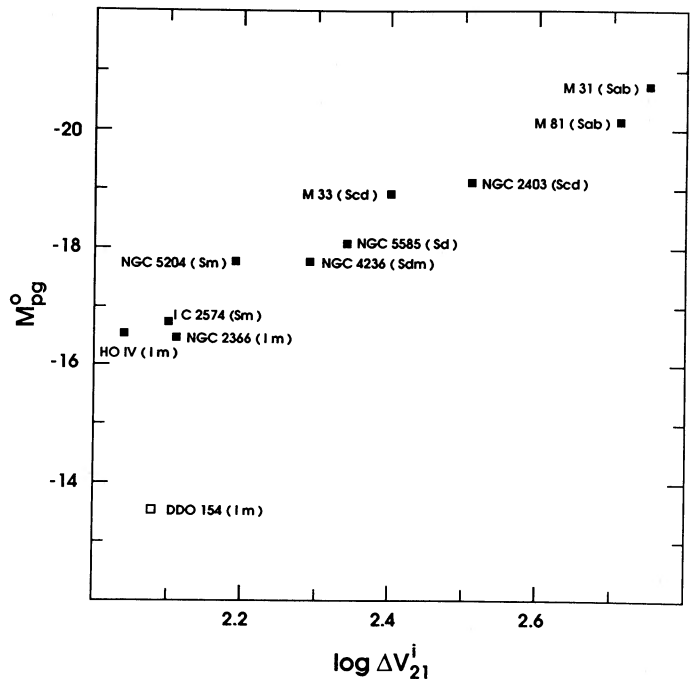


FIG. 16.—Absolute magnitude M_{pg}^0 vs. H I profile width (corrected for inclination) for a sample of nearby galaxies (filled squares) and DDO 154 (empty square).

nearby galaxies (Sandage and Tammann 1976) where the data point for DDO 154 is added. It can be seen that DDO 154 does not follow at all the relation defined by the other galaxies.

We think that this discrepancy can be explained by the fact that, in this case, $V_{\max}(\text{dark}) \approx 4V_{\max}(\text{disk})$ (see Fig. 14), while for most other galaxies we have the so-called disk-halo conspiracy (van Albada and Sancisi 1986) where $V_{\max}(\text{dark}) \approx V_{\max}(\text{disk})$. As pointed out by Milgrom and Braun (1988), the results for DDO 154 suggest that the TFR is probably more a relation between velocity and luminous (stars and gas) mass than between velocity and luminosity. If this interpretation of the TFR is correct, this means that the same situation should be observed in other dwarf systems where the maximum velocity is no more determined by the luminous disk.

Another puzzling difference is: why was there so little gas processed into stars in this system? A possible reason is that most of the H I ($r > R_{\text{H0}}$) is below the so-called "critical"

surface density of $1 \times 10^{21} \text{ cm}^{-2}$ (Skillman 1987) necessary for massive star formation to be turned on. Even if such systems are as numerous as suggested by recent studies (Tyson 1988; Dekel and Silk 1986), most of them would go undetected if most of their mass is also in such low surface density H I.

We would like to thank the Very Large Array, Kitt Peak National Observatory, and l'Observatoire astronomique du Mont Mégantic for allocation of telescope time. We thank also J. van Gorkom for her valuable assistance with the VLA observations, K. C. Freeman and G. Lake for helpful discussions, and A. F. J. Moffat for reviewing the first draft of this work. We are also grateful to J. E. Samuel for the artwork and B. Malenfant and G. Turcotte for their assistance with the OAMM observations. C. C. acknowledges financial assistance from the Natural Sciences and Engineering Research Council of Canada.

REFERENCES

- Allen, R. J., and Shostak, G. S. 1979, *Astr. Ap. Suppl.*, **35**, 163.
 Blumenthal, G. R., Faber, S. M., Flores, R., and Primack, J. R. 1986, *Ap. J.*, **301**, 27.
 Bosma, A. 1978, Ph.D. thesis, University of Groningen.
 Bothun, G. D., Impey, G. D., Malin, D., and Mould, J. R. 1987, *A.J.*, **94**, 23.
 Bottinelli, L., Gouguenheim, L., Paturel, G., and de Vaucouleurs, G. 1983, *Astr. Ap.*, **118**, 4.
 Carignan, C. 1983, Ph.D. thesis, Australian National University.
 ———. 1985, *Ap. J.*, **299**, 59.
 ———. 1987, in *IAU Symposium 117, Dark Matter in the Universe*, ed. J. Kormendy, and G. R. Knapp (Dordrecht: Reidel), p. 135.
 Carignan, C., Charbonneau, P., Boulanger, F., and Viallefond, F. 1989, submitted to *Astr. Ap.*
 Carignan, C., and Freeman, K. C. 1985, *Ap. J.*, **294**, 494.
 ———. 1988, *Ap. J. (Letters)*, **332**, L33.
 Carignan, C., Sancisi, R., and van Albada, T. S. 1988, *A.J.*, **95**, 37.
 Coleman, G. D., Wu, C.-C., and Weedman, D. W. 1980, *Ap. J. Suppl.*, **43**, 393.
 Dekel, A., and Silk, J. 1986, *Ap. J.*, **303**, 39.
 de Vaucouleurs, G. 1975, in *Stars and Stellar Systems, Vol. 9, Galaxies and the Universe*, ed. A. Sandage, M. Sandage, and J. Kristian (Chicago: University of Chicago Press), p. 557.
 ———. 1978, *Ap. J.*, **224**, 14.
 de Vaucouleurs, G., de Vaucouleurs, A., and Corwin, H. G. 1976, *Second Reference Catalog of Bright Galaxies* (Austin: University of Texas Press) (RC2).
 Hoffman, G. L., Helou, G., and Salpeter, E. E. 1988, *Ap. J.*, **324**, 75.
 Huchtmeier, W. K., and Seiradakis, J. H. 1985, *Astr. Ap.*, **143**, 216.
 Krumm, N., and Burstein, D. 1984, *A.J.*, **89**, 1319.
 Milgrom, M., and Braun, E. 1988, *Ap. J.*, **334**, 130.
 Moffat, A. F. J., Seggewiss, W., and Shara, M. M. 1985, *Ap. J.*, **295**, 109.
 Rubin, V. C., Ford, W. K., Jr., and Thonnard, N. 1980, *Ap. J.*, **238**, 471.
 Sancisi, R. 1983, in *IAU Symposium 100, Internal Kinematics and Dynamics of Galaxies*, ed. E. Athanassoula (Dordrecht: Reidel), p. 55.
 Sandage, A., and Carlson, G. 1985a, *A.J.*, **90**, 1019.
 ———. 1985b, *A.J.*, **90**, 1464.
 Sandage, A., and Tammann, G. 1976, *Ap. J.*, **210**, 7.
 Schild, R. E. 1983, *Pub. A.S.P.*, **95**, 1021.
 Skillman, E. D. 1987, in *Star Formation in Galaxies*, ed. C. J. Lonsdale (NASA Conf. Publ. 2466), p. 263.
 Skillman, E. D., Bothun, G. D., Murray, M. A., and Warmels, R. H. 1987, *Astr. Ap.*, **185**, 61.
 Skillman, E. D., Terlevich, R., Teuben, P. J., and van Woerden, H. 1988, *Astr. Ap.*, **198**, 33.
 Stetson, P. B. 1987, *Pub. A.S.P.*, **99**, 191.
 Tully, R. B. 1988, *Nearby Galaxies Catalog* (Cambridge: Cambridge University Press).
 Tully, R. B., and Fisher, J. R. 1977, *Astr. Ap.*, **54**, 661.
 Tully, R. B., Bottinelli, L., Fisher, J. R., Gouguenheim, L., Sancisi, R., and van Woerden, H. 1978, *Astr. Ap.*, **63**, 37.
 Tyson, N. D. 1988, *Ap. J. (Letters)*, **329**, L57.
 Tyson, N. D., and Scalo, J. M. 1988, *Ap. J.*, **329**, 618.
 van Albada, T. S., and Sancisi, R. 1986, *Phil. Trans. R. Soc. London*, **320**, 15.
 van Albada, T. S., Bahcall, J. N., Begeman, K., and Sancisi, R. 1985, *Ap. J.*, **295**, 305.
 Wolfe, A. M., Turnshek, D. A., Smith, A. E., and Cohen, R. D. 1986, *Ap. J. Suppl.*, **61**, 249.

SYLVIE BEAULIEU: Space Telescope Science Institute, 3700 San Martin Drive, Baltimore, MD 21218

CLAUDE CARIGNAN: Département de physique, Université de Montréal, C.P. 6128, Succ "A," Montréal, Québec, Canada, H3C 3J7